Hindawi
Journal of Chemistry
Volume 2022, Article ID 6849793, 12 pages
https://doi.org/10.1155/2022/6849793

Research Article

Synthesis, Characterization, and Photocatalytic Activity of Mixed-Ligand Cerium(III) and Bismuth(III) Complexes

Shoomaila Latif,[1] Maimoona Saeed,[2] Muhammad Imran,[2] Ayesha Javaid,[2] Uzma Hira,[1] and Liviu Mitu[3]

[1]*School of Physical Sciences, University of the Punjab, Lahore 54000, Pakistan*
[2]*Centre for Inorganic Chemistry, School of Chemistry, University of the Punjab, Lahore 54000, Pakistan*
[3]*DIMSIA Department, University of Pitesti, Pitesti 110040, Romania*

Correspondence should be addressed to Muhammad Imran; imran_inorganic@yahoo.com and Liviu Mitu; ktm7ro@yahoo.com

Received 1 August 2022; Revised 29 August 2022; Accepted 13 September 2022; Published 29 September 2022

Academic Editor: Doina Humelnicu

Two ternary complexes $(Ce(sal)_3(phen)_2)$ (1) and $(Bi(sal)_3(phen)_2)$ (2) with salicylic acid (sal) and 1,10-phenanthroline (phen) have been synthesized and characterized by analytical techniques such as UV-visible spectroscopy, FT-IR spectroscopy, PXRD, and SEM. The UV-visible study indicated the shifting of peak positions of metal complexes compared with the individual ligands whereas FT-IR analysis demonstrated that the metals were successfully coordinated with different functional groups of the ligands. The photocatalytic properties of prepared complexes were evaluated against Congo red dye as a model pollutant under ultraviolet and sunlight irradiation. The degradation efficiency of complex (2) was greater than that of complex (1). The results indicated that the investigated complexes can be employed as potential candidates for photocatalytic breakdown of synthetic dyes and can be safely recommended for environmental remediation.

1. Introduction

The uncontrolled and unmonitored dumping of dyes from different manufacturing units is a global issue which contaminates the water resources [1]. Most of the dyes are toxic and carcinogenic; therefore, their presence deteriorate the quality of water. It has been estimated by the World Bank that nearly 17–20% industrial water pollution is due to the dyeing units [2]. This increasing percentage and alarming health concerns have prompted the scientists around the globe to develop effective methods to treat the dye contaminated water. Adsorption, coagulation, sedimentation, biosorption, flocculation, and microbial degradation are some of the conventionally used methods to treat the waste water [3]. These methods are not efficient enough to completely remove the hazardous chemical substances. However, recently photocatalysis has been found to be an effective technique toward the decontamination of different pollutants in the water matrix. The practical application of photocatalysis requires a light source and a suitable catalyst for the photochemical degradation of the pollutant. Considerable efforts have been made to develop efficient photocatalysts having strong ability to degrade the pollutants of diverse origin [4]. Coordination compounds are well known as highly active catalysts capable of ensuring a high selectivity of chemical reactions [5]. The latest research studies are focusing on the synthesis of such metal complexes which can utilize solar energy, a renewable source, to photodegrade the pollutant [6–9].

The coordination complexes offer more structural flexibility than other materials because different organic ligands and metal centers can be used to obtain unique combinations. However, the type of the central metal atom, number of coordination sites, and nature of substituent group play a key role in designing their structures. Carboxylate and N-donor ligands are highly flexible and are widely used in coordination complexes [10]. Salicylic acid is an important ligand in coordination chemistry which coordinates through the

carboxylate group. It is naturally obtained from the amino acid, phenylalanine; on the other hand, it can also be synthesized artificially from sodium salicylate. Among N-donor ligands, 1,10-phenanthroline has been extensively reported and it coordinates through two pyridinic nitrogen groups [11, 12]. Sun et al. have reported the Co(II) complex with multidentate O-donor or N-donor ligands as an active catalyst against the photodegradation of methylene bluehttps://www.sciencedirect.com/topics/chemistry/methylene-blue, methyl violet, orange G, and rhodamine B [13]. Recently, Naik et al. reported the coordination complexes of Ni (II) with N-donor (imidazole) and O-donor (4-nitrobenzene) ligands for the photocatalytic removal of Amaranth dye [14]. Ortiz–Zarco et al. have also reported the Fe(III) complex for the photodegradation of Rhodamine B [15]. It is established in literature that heavier *p* block and *f* block elements have been relatively less explored for various applications. Among these blocks, bismuth and cerium are potential candidates due to their flexible coordination numbers, strong spin orbit coupling constant, easy handling, and relatively less toxic, especially in case of bismuth when compared to its neighbors i. e. thallium and lead. Cerium exhibits excellent features like optical properties, good electrical conductivity, high diffusivity, and thermal stability [16]. There are numerous bismuth compounds which have been reported for the degradation of dyes including oxides, oxyhalides, vanadates, ferrites, molybdates, and its different nanohybrids [17–20]. Similarly, cerium is another emerging candidate in this respect [21].

Keeping in view these characteristics of bismuth and cerium, in this paper, we describe the structure/morphology of two complexes of Ce(III) and Bi(III). Their photocatalytic behavior toward Congo red dye as a model pollutant is also a part of this manuscript.

2. Experimental Methods

2.1. Materials. Cerium chloride heptahydrate (98%), bismuth nitrate pentahydrate (98%), salicylic acid (99%), 1,10-phenanthroline monohydrate (99%), and sodium bicarbonate (99%) were used and supplied by Sigma Aldrich. Congo red (CR), ethanol, dimethyl sulfoxide (DMSO), and dimethylformamide (DMF) were obtained from Merck. Optical properties of the complexes were analyzed by a UV-Visible spectrophotometer (T90+ UV-VIS spectrophotometer Perkin Elmer λ–35, Waltham, MA, USA) in the range of 200–400 nm. FT-IR analysis was performed using a FT-IR-4100 type spectrophotometer in the range of 4000–650 cm^{-1}. The structural properties of the obtained products were characterized by an X-ray diffractometer (XRD-Shimadzu XD-3A), and surface morphologies were observed using a scanning electron microscope (VEGA3 TESCAN) employed at an accelerating voltage of 12.5 kV. The thermal stability of the prepared complexes was analyzed by a thermogravimetric analyzer (PerkinElmer Diamond Series unit, USA).

2.2. Synthesis of Cerium(III) and Bismuth(III) Complexes. The mixed ligand complexes of Cerium(III) and Bismuth(III) were fabricated by reacting the metal precursor solution with the mixture of ligands following the procedure reported by Gao et al., with slight modifications [22]. The ligand solution was synthesized by taking salicylic acid (0.0621 g, 0.03 mol) and 1,10-phenanthroline (0.5406 g, 0.02 mol) in anhydrous ethanol solution (15 mL). 15 mL of $CeCl_3.7H_2O$ (0.0558 g, 0.01 mol) was added drop wise in the aforementioned solution of ligands. The aqueous solution of $NaHCO_3$ (0.0378 g, 0.03 mol) was added dropwise in the prepared solution while stirring vigorously. The resulting mixture was refluxed for 1 h at 70°C with continuous stirring. The obtained solution was filtered and slowly evaporated at 25°C for two days to get mustard yellow precipitates of $(Ce(sal)_3(phen)_2)$, complex (1). The second complex was synthesized following the same procedure using bismuth nitrate (0.0727 g, 0.01 mol), and the bright white precipitates of $(Bi(sal)_3(phen)_2)$, complex (2) were obtained. The general synthetic route of two complexes is given in (Scheme 1).

2.3. Photocatalytic Study. Photocatalytic activity of synthesized metal complexes was studied against the Congo red dye. Each complex (10 mg) was added in the solution of Congo red dye (10 mg/L, 50 mL) and stirred for one hour under dark conditions. The absorbance of the sample was noted at $\lambda_{max} = 498$ nm using a UV-visible spectrophotometer; then, the solution was irradiated with a 6 W UV-A lamp with photon flux density of 3.12×10^{-8} einstein cm^{-2} s^{-1}. The absorbance of dye solution was recorded after each 30 min interval and photocatalytic activity was determined in terms of percentage degradation using the mathematical expression (equation (1)).

$$\text{Degradation}\,(\%) = \left[\frac{A_o - A_t}{A_o}\right] \times 100, \tag{1}$$

where A_o is the initial absorbance of Congo red solution, whereas A_t denotes absorbance at specific interval of time [17].

The optimization of different photocatalytic parameters were also carried out for complexes (1) and (2). The effect of initial concentration of dye, catalyst dosage, pH, temperature, and light irradiation time were studied. The photocatalytic experiment was also carried out in sunlight (sunny day of August, 11 am-2 pm) to investigate the photocatalytic activity of complexes (1) and (2) under natural light.

The recyclability of the catalyst is an important parameter to investigate the stability of the catalyst. The catalyst was recovered after its first use through centrifugation, washed thoroughly with water, and oven-dried at 60°C. The recovered catalyst was reused for the photocatalytic degradation of Congo red.

3. Results and Discussion

The synthesized complexes were subjected to various analytical techniques to analyze their structural and morphological features.

3.1. FT-IR Analysis. The FT-IR spectra were recorded in the range of 4000–650 cm^{-1} and provided valuable insights

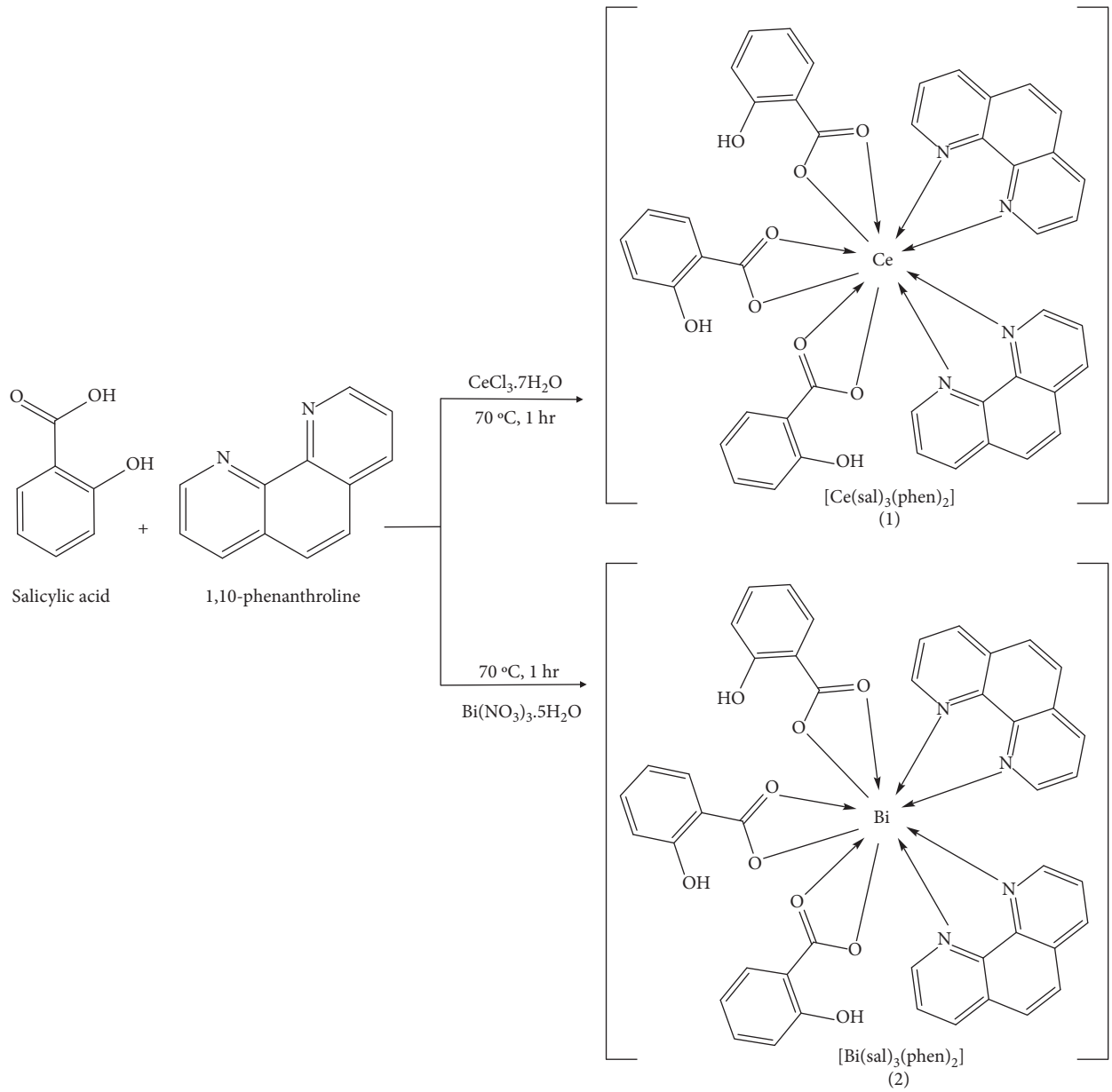

Scheme 1: General synthetic route of $(Ce(sal)_3(phen)_2)$, (1) and $(Bi(sal)_3(phen)_2)$, (2) complexes.

about the coordination of functional groups in the prepared complexes. The FT-IR spectra of complexes (1) and (2) were compared with the FT-IR spectra of salicylic acid and 1,10-phenanthroline in order to find their involvement in the metal complexes. According to the IR absorption spectra, the structure of the complexes showed the peaks of different functional groups. Figure 1 shows that the stretching vibrations of carbonyl (C=O) group at 1665 cm^{-1} for salicylic acid has been red-shifted to 1630 cm^{-1} with reduced intensity in the synthesized complexes, revealing that the oxygen of the ligand coordinated with the Ce and Bi metals in complexes (1) and (2), respectively [22]. The peak that appeared around 1437 to 1450 cm^{-1} for (1) and (2) was ascribed to the stretching vibrations of (−C=N) suggesting that the N atoms of the 1,10-phenanthroline has successfully coordinated with the metal atoms in both complexes [23]. It has also been observed that stretching vibrations due to the C–H groups of 1,10-phenanthroline (740 cm^{-1} and 807 cm^{-1}) and salicylic acid (736 cm^{-1} and 850 cm^{-1}) disappeared and some new peaks appeared at 720 cm^{-1}, 753 cm^{-1}, and 862 cm^{-1} in our complexes which is found to be in agreement with the reported literature [24]. Moreover, symmetric and asymmetric stretching vibrations of–COOH group of salicylic acid appearing at 1345 cm^{-1} has shifted to 1449 cm^{-1} upon the formation of the complexes. As established from the literature, this shifting indicates the formation of bond between oxygen atom of carboxyl functional group and metal atoms [25, 26]. The absence of stretching vibrations of hydroxyl and nitrate groups in complexes (1) and (2) indicated the purity of synthesized complexes [22].

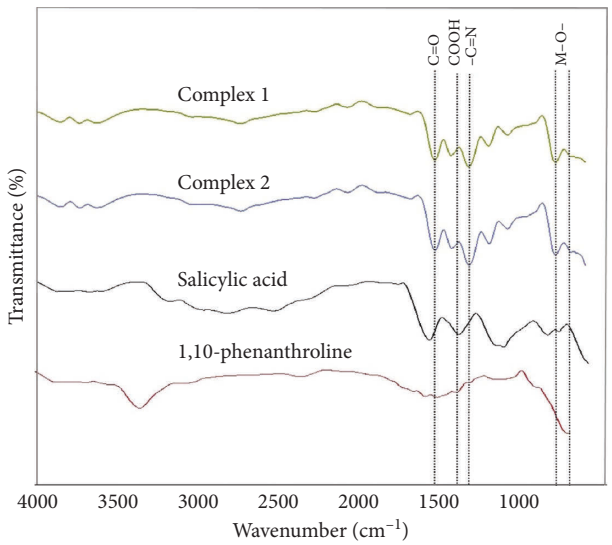

Figure 1: The FT-IR spectra of 1, 10-phenanthroline, salicylic acid, complexes (1) and (2).

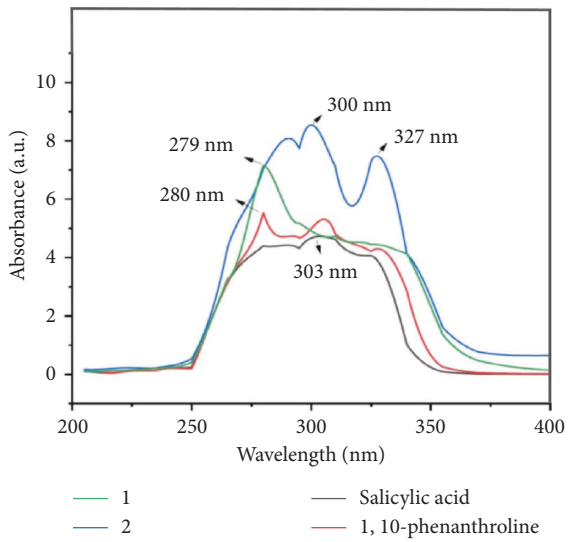

Figure 2: UV-visible absorption spectra of salicylic acid, 1,10-phenanthroline. Complex (1) and (2).

3.2. UV-Visible Spectroscopy. The optical properties of the prepared complexes were analyzed through UV–visible spectroscopy. The absorption spectra of the ethanolic solutions of (1) and (2) were obtained in the wavelength range of 200–400 nm (Figure 2). It is evident that the characteristic peaks of 1,10-phenanthroline and salicylic acid appeared in the UV range at 280 nm and 303 nm, respectively, and were allocated to the $\pi \longrightarrow \pi^*$ transitions of aromatic ring of the ligands [23]. The complex (1) has shown a characteristic peak at 279 nm indicating a slight blue shift compared with the main peak of 1,10-phenanthroline around 280 nm, owing to the coordination of nitrogen atoms of 1,10-phenanthroline with cerium metal [24]. Although, the absorption spectrum of the complex (1) has a prominent absorption peak of 1,10-phenanthroline but a very small shoulder peak of salicylic acid around 300 nm shows the coordination of both ligands with metal atoms [25]. The complex (2) shows two absorption peaks, one main peak at 327 nm with a shoulder peak of 300 nm [27]. The red shifting of ligand peaks in complex (2) reflects the bathochromic effect and is also an indication for the metal-ligand coordination. The results of our study are in accordance with the reported absorption peaks of the 1,10-phenanthroline and salicylic acid at 280, 305, 330 nm and 265, 303, 320 nm, respectively, with slight shifting in their positions after coordinating with the metal [26].

The UV-vis data were used to evaluate the band gap energy of the catalysts using Tauc's plot method (equation (2)) [28].

$$(\alpha h\nu)^{n} = k\left(h\nu - E_g\right), \tag{2}$$

where α, h, ν, k,E_g, and n represent the absorption coefficient, Planck's constant, frequency, probability parameter for the transition, the optical band gap, and type of electronic transition, respectively. The value of $n = 2$ was used for direct allowed transitions. The graph was plotted between energy at x-axis and $(\alpha h\nu)^2$ at y-axis. The value of optical band gaps

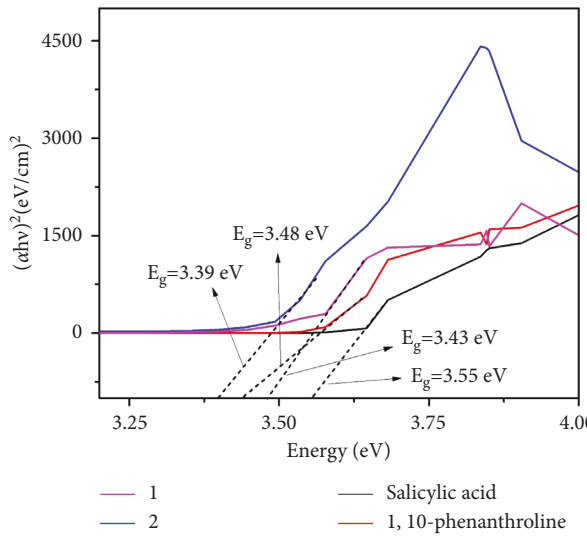

Figure 3: Tauc's plots of salicylic acid, 1,10-phenanthroline, complex (1) and (2) for the estimation of band gap energy.

were obtained by extrapolation of the linear part of the curve (Figure 3). Tauc's plots revealed semiconducting behavior of the complexes. The complex 1 has shown the optical band gap of 3.48 eV, and complex 2 has shown the value of 3.39 eV. It has been established in the literature that a narrow band gap is associated with the better photocatalytic performance [29].

3.3. X-Ray Diffraction Analysis (XRD). The crystal structures of the complex (1) and (2) were analyzed from the data of X-ray diffractograms obtained at room temperature (Figure 4). Different characteristic peaks of cerium and bismuth complexes were observed at the angle 2θ in the range of 10–80°. The appearance of well-defined sharp peaks revealed

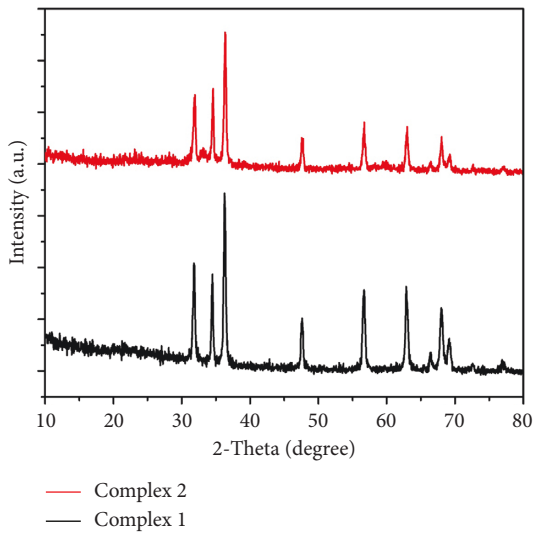

Figure 4: XRD patterns of complexes (1) and (2).

the crystalline nature of the synthesized complexes. The main diffraction peaks were appeared at 31.70°, 34.51°, 36.30°, 47.45°, 56.50°, 62.88°, and 67.88° indexed to the diffraction planes of (311), (221), (110), (113), (222), (211), and (331), respectively. The obtained XRD patterns were compared to the reported patterns of salicylic acid (JCPDS card no. 14–0882) and 1,10-phenanthroline (JCPDS card no. 29–1839) [30, 31]. It has been observed that the peak position and intensity of the diffraction peaks in the complexes were slightly different from the reported patterns of the ligands. This variation indicated the coordination of the metal with the functional groups of the ligands [32, 33]. Moreover, the disappearance of some ligand peaks has also been observed along with the emergence of some new peaks, thus confirming the successful synthesis of metal complexes, and it is in accordance with the reported literature [30, 31, 34]. The crystallite size (D) of the synthesized complexes (1) and (2) was calculated with the Scherer formula (equation (3)).

$$D = (k\lambda)/(\beta \cos \theta), \quad (3)$$

where k, λ, β, and θ represent Scherer's constant (0.9), wavelength of the X-ray (0.154 nm), the full width of peak at half maxima (FWHM), and Bragg's angle, respectively. The mean crystallite size for the Ce(III) complex was calculated to be 15.3 nm while for Bi(III) complex was 19.5 nm using Debye Scherer's equation.

3.4. Scanning Electron Microscopy (SEM). SEM illustrations were obtained to observe the surface morphology of synthesized metal complexes (1) and (2). The Ce(III) complex demonstrated accumulated and irregularly dispersed cuboid-rod shaped particles of various sizes (Figure 5, 5(a) and 5(b)), while on the other hand, Bi(III) complex showed a heaped distribution of diamond shaped lumps as represented in (Figure 5, 5(c) and 5(d)). Presumably, the high synthesis temperature leads to increased energy; therefore, particles aggregate with each other to yield large shaped morphology [16]. Both complexes revealed distinguishable morphology from each other with slight spongy nature which can be advantageous for the adsorption of pollutant molecules onto the surface of the catalyst [25, 35].

3.5. Thermogravimetric Analysis (TGA). The stability of the synthesized complexes was determined through thermogravimetric analysis (TGA) in the temperature range of 23 to 1000°C (Figure 6). The TGA curve of complex 1 was found to be stable up to 239°C, whereas complex 2 showed stability up to 210°C. Afterward, the decomposition process set in with two distinct decomposition steps. The first weight loss of 50.2% and 39.3% was observed in the temperature range of 239–412°C for complex 1 and complex 2, respectively. The observed weight losses were ascribed to the removal of organic ligands due to the combustion [36]. The removal of ligands continued, and another weight loss of 8.1% was observed for complex 1 in the temperature range of 412–570°C, and complex 2 showed *ca.* 6.4% weight loss in the temperature range of 412–650°C. Such type of weight loss with two distinct degradation steps is in well agreement with the recent study of Huang et al., where two step weight loss was reported for the removal of organic ligands from the bismuth(III) complex ((1,10-phen)$Bi(C_2O_4)_{1.5}$) [37]. The TGA curve became stable after 570°C for complex 1 and 650°C for complex 2; no further weight losses indicated the stability of the residues due to the formation of corresponding metal oxides [38]. The high thermal decomposition temperature indicated good thermal stability of the complexes due to the highly polarized M-O bonds [39]. Moreover, the high stability temperature of complex 2 with overall small weight loss compared to the complex 1 indicated that complex 2 was more stable than complex 1.

3.6. Photocatalytic Degradation Studies. The photocatalytic degradation of fabricated complexes was studied against Congo red as a model pollutant. Figure 7 shows that there was a negligible degradation rate when the solution of dye was exposed to UV light for 120 min indicating the high stability of the dye. However, the addition of synthesized metal complexes appreciably enhanced the degradation efficiency. It was noticed that the percentage degradation was 83% using complex (1); whereas, for complex (2), the degradation efficiency reached up to 92% within 120 min. The slight difference in the photocatalytic behavior of complex (1) and (2) was attributed to the different nature of the central metal atoms. These results were supported by the relevant literature, for instance, Sangsefidi et al. reported the degradation efficiency ≈90% for cerium complexes against azo dyes [16]. Likewise, Tan et al. reported the degradation efficiency ≈99% against Rhodamine B dye using {(Hphen)$(BiCl_4)_n$} complex [38]. Table 1 compares the photocatalytic efficiencies of different reported complexes against the degradation of Congo red.

3.7. Optimization of Photocatalytic Parameters

3.7.1. Effect of Initial Concentration of the Dye. The influence of initial concentration of dye was studied by changing the

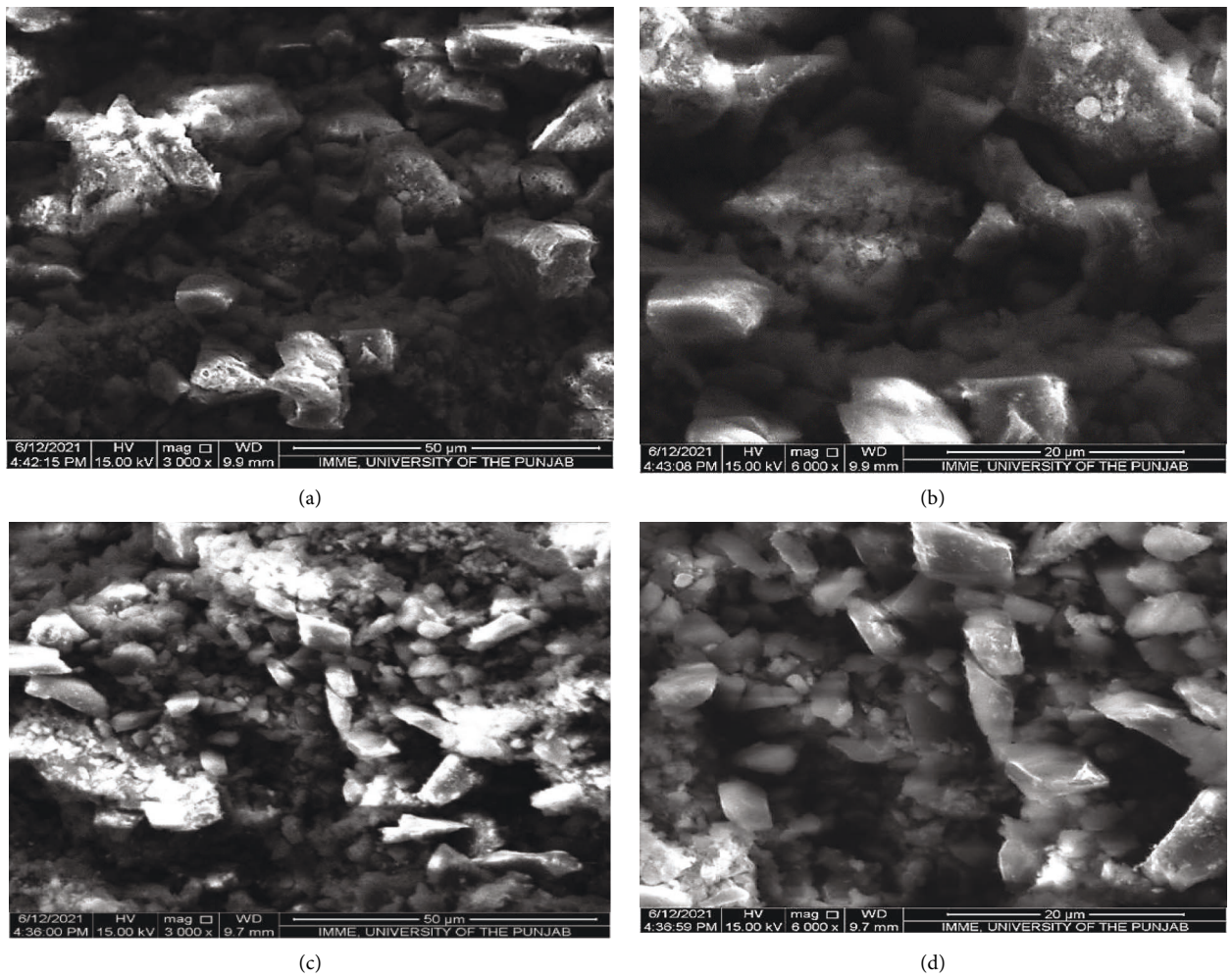

Figure 5: SEM micrographs of (a and b) complex (1), (c and d) complex (2) at different resolutions.

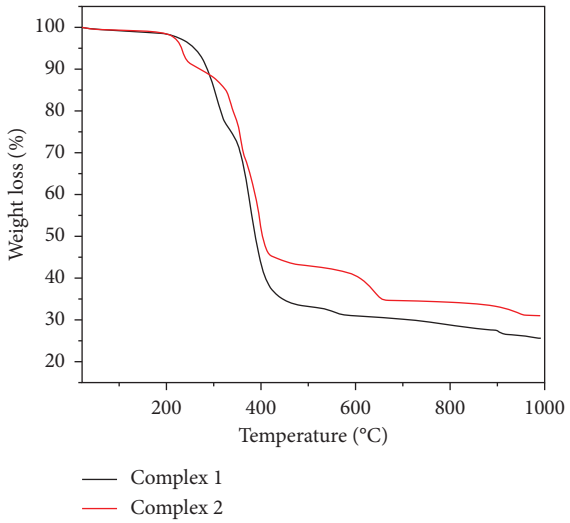

Figure 6: Thermogravimetric curves of complex 1 and complex 2.

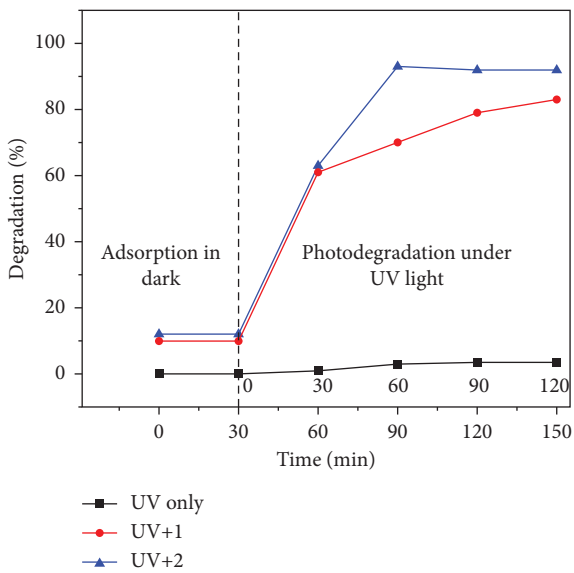

Figure 7: Degradation efficiency of complexes (1) and (2) against Congo red dye under UV light irradiation.

Table 1: Comparison of the photocatalytic activities of different reported complexes with the synthesized complexes against the degradation of Congo red.

Type of catalyst	Pollutant	Catalyst amount	Dye concentration	Light source	Photocatalytic capacity (%)	Irradiation time (min)	References
$\{(Cd_2(H_2O)\ (tpeb)_2(1,2\text{-}chdc)_2).H_2O\}_n$	Congo red	12 mg	200 mg/L	196 W xenon lamp	90	90	[10]
Cu(II)/Guanidine functionalized disiloxane complex	Congo red	50 mg	200 mg/L	400 W sodium lamp	97	50	[40]
Copper(II) complex from bis-(2-pyridylmethyl)amine NNN-derivative ligands	Congo red	5×10^{-4} mol/L	3.3×10^{-5} mol/L	250 W Hg-vapour lamp	100	90	[41]
$\{(Co_3(BTC)_2(Bimb)_{2.5}) \bullet 2H_2O\}_n$	Congo red	10 mg/L	0.01 mmol	UV irradiation	15.8	135	[42]
$(Bi(sal)_3(phen)_2)$ $(Ce(sal)_3(phen)_2)$	Congo red	10 mg	10 mg/L	UV irradiation	92 83	120	This work

tpeb = 1,3,5-tri-4-pyridyl-1,2-ethenylbenzene. CHDC = 1,2-cyclohexanedicarboxylic acid. Bimb = 1,4-bis ((1H-imidazole-1-yl)methyl) benzene. H_3BTC = 1,3,5-benzenetricarboxylic acid.

concentration of Congo red in the range of 5 mg/L to 30 mg/L at neutral pH and catalyst dose of 10 mg. It was observed that when concentration of dye was increased from 5 mg/L to 10 mg/L, the degradation efficiency was enhanced from 66% to 69% for complex (1), and 68% to 72% for complex (2) (Figure 8(a)). When dye concentration was further increased (15 mg/L, 20 mg/L, 25 mg/L, 30 mg/L), it was observed that degradation efficiency decreased gradually for both complexes. This behavior is explained by the fact that initially when dye concentration was increased, there were sufficient catalytic sites present for the dye molecules to get adsorb and degraded by the catalyst. However, when it is further increased, the presence of large amount of dye particles compete for the surface of the catalyst which in turn reduces the availability of free radicals to the dye molecule; therefore, degradation of the dye is prevented [38]. Another contributing factor toward the reduced degradation efficiency is that photons may be interrupted to reach the surface of the photocatalyst when higher concentrations of dye are used [43].

3.7.2. Effect of Catalyst Dose. The influence of catalyst dosage on the dye degradation was examined by using different doses of catalyst (10 mg-60 mg) and other parameters were kept constant. It has been noticed that the percentage degradation first increased by increasing the catalyst dose owing to the availability of numerous active sites on the catalyst surface (Figure 8(b)). These large number of catalytic sites generated more free radicals for the dye degradation. When catalyst dose was further increased, a decrease in the percent degradation was observed due to less penetration of photons caused by the light scattering effect [44, 45]. In addition, the high dose of catalyst also increases the collision frequencies between activated and ground state molecules leading to the agglomeration of the catalyst, thereby reducing the active sites of the catalyst [46].

3.7.3. Effect of pH. The photocatalytic activity of the two complexes was studied at various pH (3–9) while keeping the optimum dye concentration and catalyst dose. As evident from the (Figure 8(c)), both complexes have shown similar trend. The maximum degradation of dye was observed at neutral pH, whereas decreased activity was observed in acidic and basic media. Based on the established presumption, the agglomeration of catalyst takes place in acidic conditions (below pH = 6) which leads to the decreased surface area, and hence less active sites. In case of basic conditions, the surface of the catalyst may become negatively charged due to excess hydroxyl ions, which repel the anionic Congo red dye [45, 47].

3.7.4. Effect of Temperature. The effect of varying temperature was studied on the photocatalytic properties of the complexes. As shown in (Figure 8(d)), the photocatalytic degradation efficiency increases by increasing the temperature. The maximum catalytic efficiency was observed at 333 K with a degradation percentage of 75% and 77% for complex (1) and complex (2), respectively. This could be due to the increase in the collisions of the reactant molecules by increasing the temperature which in turn enhance the reaction rate [48, 49]. When temperature was further increased up to 343 K, the rate of photocatalytic reaction decreased due to the enhanced recombination of charge carriers [50].

3.7.5. Effect of Time. Figure 8(e) shows the effect of irradiation time on the photodegradation of Congo red. It can be seen that initially, degradation efficiencies were 50% and 58% for complex (1) and complex (2), respectively, in only first 5 min of irradiation. This is because in the early stages of reaction, there are numerous active sites which instantly degrade the pollutant by producing several free radicals. Although maximum degradation was achieved in 35–40 min of irradiation for both complexes, but this time the degradation rate was not as abrupt as in the first 5 min of light exposure. The slow rate of reaction after certain time is due to the competition between reactants and intermediates for the availability of the free radicals. When reaction medium was further exposed to light (up to 60 min), almost constant percent degradation was observed because it is assumed that at this stage, the intermediate products start depositing on

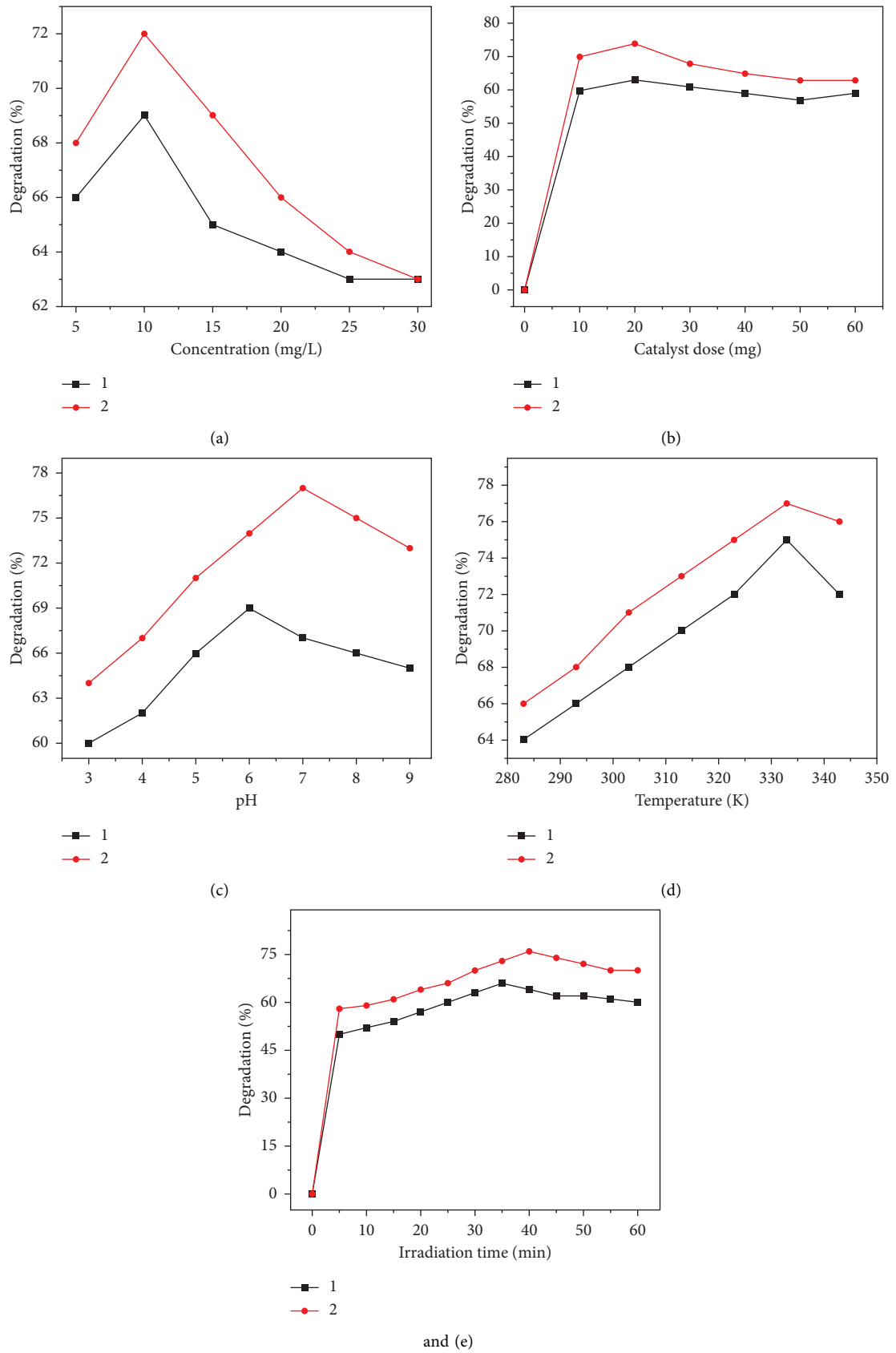

Figure 8: Effect of various photocatalytic parameters. (a) Initial concentration of dye, (b) catalyst dose, (c) pH, (d) temperature, and (e) irradiation time on (c) the degradation efficiency of complexes (1) and (2).

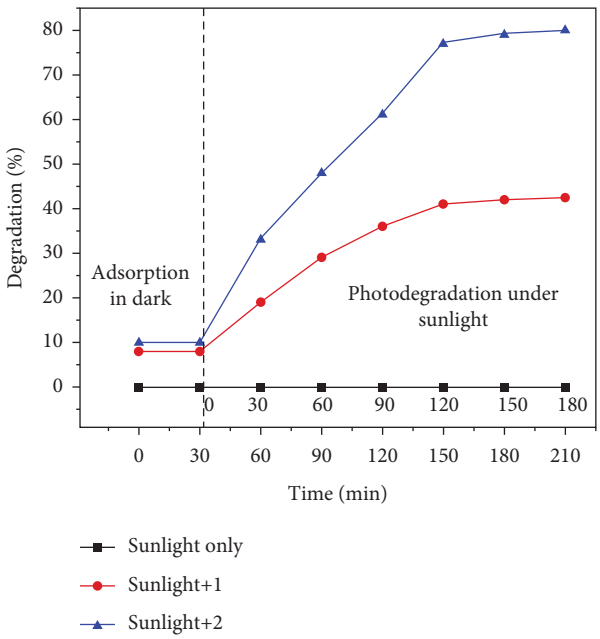

Figure 9: Degradation efficiencies of complexes (1) and (2) against Congo red under solar light irradiation.

the catalyst surface, and no more active sites remain available for catalytic activity [31, 51].

3.8. Photocatalytic Activity under Solar Light Irradiation. The degradation efficiencies of complexes (1) and (2) were also analyzed in the presence of sunlight. Initially, the dye solution was exposed to sunlight only and no degradation was observed. However, the addition of the Ce(III) complex has led to 19% and the Bi(III) complex led to 33% degradation in first 30 min of light exposure, and there was a continuous improvement in the degradation performance as a function of time (Figure 9). The degradation efficiencies reached 42% for the Ce(III) complex and 80% for the Bi(III) complex in 180 min only. These results were in agreement with the reported literature where bismuth complexes have been reported for the effective photocatalytic activities against azo dyes under solar light [52].

3.9. Photodegradation Mechanism. The plausible mechanism for the abovementioned photocatalytic reaction can be proposed as per the existing literature [53]. The photocatalytic reaction starts when light is exposed on the surface of the photocatalyst. The energy from the light photons causes the transfer of electrons from the highest occupied molecular orbital (HOMO) of the catalyst to the lowest unoccupied molecular orbital (LUMO). This migration results in the formation of holes in the HOMO and electrons in the LUMO (equation (4)). The positive holes react with water molecules and produce hydroxyl radicals (equation (5)). On the other hand, electrons react with dissolved oxygen to yield superoxide radicals (equation (6)). The superoxide radicals may further react with protons to yield hydrogen peroxide (H_2O_2) which produces hydroxyl

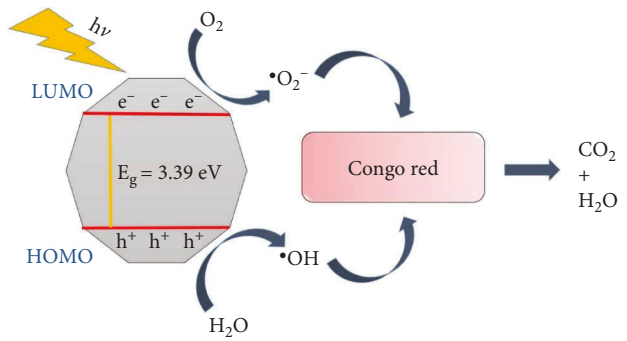

Figure 10: The plausible mechanism of the photodegradation of Congo red under UV light irradiation using complex 2.

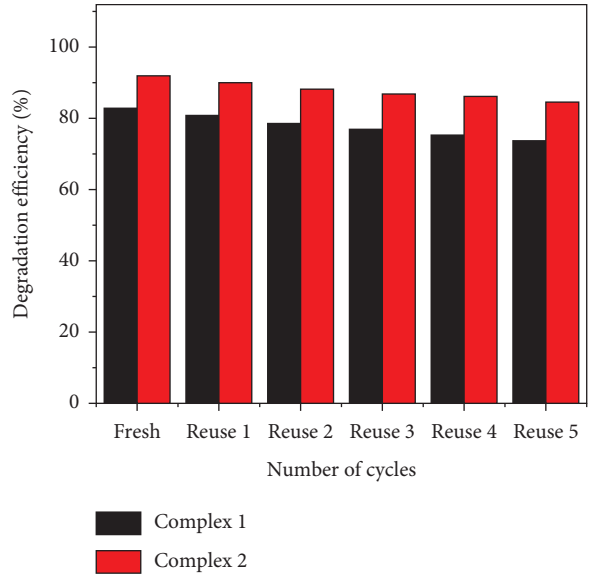

Figure 11: Reusability of the complex 1 and 2 under UV light irradiation.

radicals (•OH) upon dissociation (equations (7)–(9)). Thus, a series of redox reactions produce reactive radicals on the surface of the catalyst which are powerful oxidizing agents and attack the dye molecules and finally yield small less toxic degradation products such as carbon dioxide and water (equations (10) and (11)). Figure 10 represents the general mechanism of the photocatalytic activity of the complex 2 against Congo red.

$$\text{Complex } 2 + h\nu \longrightarrow h^{+}_{\text{HOMO}} + e^{-}_{\text{LUMO}}, \quad (4)$$

$$h^{+}_{\text{HOMO}} + H_2O \longrightarrow OH^{\bullet} + H^{+}, \quad (5)$$

$$e^{-}_{\text{LUMO}} + O_2 \longrightarrow {\bullet}O_2^{-}, \quad (6)$$

$${\bullet}O_2^{-} + H_2O \longrightarrow HO_2^{\bullet}, \quad (7)$$

$$2HO_2^{\bullet} \longrightarrow H_2O_2 + O_2, \quad (8)$$

$$e^{-}_{\text{LUMO}} + H_2O_2 \longrightarrow OH^{\bullet}, \quad (9)$$

$$OH^{\bullet} + \text{Congo red} \longrightarrow \text{Degradation products}, \quad (10)$$

$$\bullet O_2^- + \text{Congo red} \longrightarrow \text{Degradation products}. \quad (11)$$

3.10. Reusability of the Complexes. The stability of the complexes 1 and 2 was studied in terms of repeated use of the complexes as catalysts under similar conditions of photocatalytic reaction against Congo red. Figure 11 shows that complex 1 and 2 were stable even after five runs of photocatalytic activity with photocatalytic activities reaching 74% and 84.7%, respectively. The complex 1 has shown 9% loss of photoactivity after 5^{th} reuse, whereas complex 2 has shown only 7.3% loss of photocatalytic efficiency revealing its greater stability and potential to be used again and again.

4. Conclusions

The Ce(III)- and Bi(III)-based mixed ligand ternary complexes were synthesized by the solution technique, employing salicylic acid and 1,10-phenanthrolie as ligands. The formation of Ce(III) and Bi(III) complexes were confirmed by UV–visible spectroscopy, FT-IR spectroscopy, XRD, and SEM techniques. The photocatalytic efficiency of the Bi(III) complex against Congo red was found to be higher (92%) compared with the Ce(III) complex (83%) under UV light irradiation, which is attributable to the smaller band gap of the Bi(III) complex (3.39 eV) than the Ce(III) complex (3.48 eV). The reusability of the catalyst suggested its stability with a small loss of photocatalytic activity even after five runs. Furthermore, the satisfactory photocatalytic activity (80%) of the Bi(III) complex under sunlight indicated its potential to be used as a cost-effective photocatalyst to remove pollutants.

Data Availability

All related data are mentioned in the manuscript with references.

Conflicts of Interest

The authors declare that they have no conflicts of interest.

Acknowledgments

The authors express gratitude to the University of the Punjab, Lahore, Pakistan, for financial support. The authors are thankful to the home department for funding this work.

References

[1] M. R. Islam and M. G. Mostafa, "Textile dyeing effluents and environment concerns-a review," *Journal of Environmental Science and Natural Resources*, vol. 11, no. 1-2, pp. 131–144, 2019.

[2] S. H. S. Chan, T. Yeong Wu, J. C. Juan, and C. Y. Teh, "Recent developments of metal oxide semiconductors as photocatalysts in advanced oxidation processes (AOPs) for treatment of dye waste-water," *Journal of Chemical Technology and Biotechnology*, vol. 86, no. 9, pp. 1130–1158, 2011.

[3] G. Crini and E. Lichtfouse, "Advantages and disadvantages of techniques used for wastewater treatment," *Environmental Chemistry Letters*, vol. 17, no. 1, pp. 145–155, 2019.

[4] A. Javaid, S. Latif, M. Imran et al., "Nanohybrids-assisted photocatalytic removal of pharmaceutical pollutants to abate their toxicological effects-A review," *Chemosphere*, vol. 291, Article ID 133056, 2022.

[5] C. Y. Yue, X. W. Lei, Y. F. Han et al., "Transition-metal-complex cationic dyes photosensitive to two types of 2D layered silver bromides with visible-light-driven photocatalytic properties," *Inorganic Chemistry*, vol. 55, no. 23, pp. 12193–12203, 2016.

[6] A. Djebli, A. Boudjemaa, H. Bendjeffal et al., "Photocatalytic degradation of methyl orange using $Zn[Fe(CN)_5NO]$ complex under sunlight irradiation," *Inorganic and Nano-Metal Chemistry*, vol. 50, no. 11, pp. 1115–1122, 2020.

[7] P. Hayati, Z. Mehrabadi, M. Karimi et al., "Photocatalytic activity of new nanostructures of an Ag(I) metal-organic framework (Ag-MOF) for the efficient degradation of MCPA and 2, 4-D herbicides under sunlight irradiation," *New Journal of Chemistry*, vol. 45, no. 7, pp. 3408–3417, 2021.

[8] A. Kuila, R. Maity, P. Acharya et al., "Significant photodegradation of carcinogenic organic dyes by a 1D supramolecular heteroleptic Cu(ii) complex under sunlight irradiation," *New Journal of Chemistry*, vol. 46, no. 24, pp. 11804–11811, 2022.

[9] M. Rani and U. Shanker, "Insight in to sunlight-driven rapid photocatalytic degradation of organic dyes by hexacyanoferrate-based nanoparticles," *Environmental Science and Pollution Research*, vol. 28, no. 5, pp. 5637–5650, 2021.

[10] J. G. Zhang, W. J. Gong, Y. S. Guan, H. X. Li, D. J. Young, and J. P. Lang, "Carboxylate-assisted assembly of zinc and cadmium coordination complexes of 1, 3, 5-tri-4-pyridyl-1, 2-ethenylbenzene: structures and visible-light-induced photocatalytic degradation of Congo red in water," *Crystal Growth & Design*, vol. 18, no. 10, pp. 6172–6184, 2018.

[11] L. Moráň, T. Pivetta, S. Masuri et al., "Mixed copper(II)-phenanthroline complexes induce cell death of ovarian cancer cells by evoking the unfolded protein response," *Metallomics*, vol. 11, no. 9, pp. 1481–1489, 2019.

[12] G. A. Lawrance, *Introduction to Coordination Chemistry*, John Wiley & Sons, Hoboken, NJ, USA, 2013.

[13] H.-Y. Sun, C.-B. Liu, Y. Cong, M.-H. Yu, H.-Y. Bai, and G.-B. Che, "New photocatalyst for the degradation of organic dyes based on $(Co_2$ (1, 4-BDC)$(NCP)_2)_n$ $4nH_2O$," *Inorganic Chemistry Communications*, vol. 35, pp. 130–134, 2013.

[14] A. P. Naik, J. V. Sawant, H. Mittal, A. Al Alili, and P. P. Morajkar, "Facile synthesis of 2D nanoflakes and 3D nanosponge-like Ni1-xO via direct calcination of Ni (II) coordination compounds of imidazole and 4-nitrobenzoate: adsorptive separation kinetics and photocatalytic removal of Amaranth dye contaminated wastewater," *Journal of Molecular Liquids*, vol. 325, Article ID 115235, 2021.

[15] E. Ortiz-Zarco, D. Solis-Casados, L. Escobar-Alarcón, and I. García-Orozco, "Visible light-driven photocatalyst: an iron (III) coordination compound in Rhodamine B degradation," *Journal of Photochemistry and Photobiology A: Chemistry*, vol. 424, Article ID 113629, 2022.

[16] F. S. Sangsefidi, M. Sabet, and M. Salavati-Niasari, "Synthesis and characterization of ceria nanostructures with different morphologies via a simple thermal decompose method with different cerium complexes and investigation the

photocatalytic activity," *Journal of Materials Science: Materials in Electronics*, vol. 27, no. 8, pp. 8793–8801, 2016.

[17] Z. Wang, M. Chen, D. Huang et al., "Multiply structural optimized strategies for bismuth oxyhalide photocatalysis and their environmental application," *Chemical Engineering Journal*, vol. 374, pp. 1025–1045, 2019.

[18] A. P. Reverberi, P. S. Varbanov, M. Vocciante, and B. Fabiano, "Bismuth oxide-related photocatalysts in green nanotechnology: a critical analysis," *Frontiers of Chemical Science and Engineering*, vol. 12, no. 4, pp. 878–892, 2018.

[19] M. Usman, M. Humayun, S. S. Shah et al., "Bismuth-graphene nanohybrids: synthesis, reaction mechanisms, and photocatalytic applications-a review," *Energies*, vol. 14, no. 8, p. 2281, 2021.

[20] A. Tariq, S. I. Ali, D. Akinwande, and S. Rizwan, "Efficient visible-light photocatalysis of 2D-MXene nanohybrids with Gd3+ and Sn4+ codoped bismuth ferrite," *ACS Omega*, vol. 3, no. 10, pp. 13828–13836, 2018.

[21] H. Yang, L. Jia, Z. Zhang et al., "Novel cerium-based MOFs photocatalyst for photocarrier collaborative performance under visible light," *Journal of Catalysis*, vol. 405, pp. 74–83, 2022.

[22] J. Gao, Q. Huang, Y. Wu, Y. Q. Lan, and B. Chen, "Metal-organic frameworks for photo/electrocatalysis," *Advanced Energy and Sustainability Research*, vol. 2, no. 8, Article ID 2100033, 2021.

[23] C. J. Xu, H. Yang, F. Xie, and X. Z. Guo, "Photoluminescence enhancement of Sm3+ in the Sm3+ salicylic acid o-phenanthroline ternary composite," *Journal of Alloys and Compounds*, vol. 392, no. 1-2, pp. 96–99, 2005.

[24] D. M. Prabaharan, K. Sadaiyandi, M. Mahendran, and S. Sagadevan, "Structural, optical, morphological and dielectric properties of cerium oxide nanoparticles," *Materials Research*, vol. 19, no. 2, pp. 478–482, 2016.

[25] G. Sharma and A. K. Narula, "Eu3+, Yb3+ and Eu3+-Yb3+ complexes with salicylic acid and 1,10-phenanthroline: synthesis, photoluminescent properties and energy transfer," *Journal of Fluorescence*, vol. 25, no. 2, pp. 355–360, 2015.

[26] C. Q. Shen, T. L. Yan, Y. T. Wang, Z. J. Ye, C. J. Xu, and W. J. Zhou, "Synthesis, structure and luminescence properties of binary and ternary complexes of lanthanide (Eu^{3+}, Sm^{3+} and Tb^{3+}) with salicylic acid and 1, 10-phenanthroline," *Journal of Luminescence*, vol. 184, pp. 48–54, 2017.

[27] L. John, R. S. Joseyphus, and I. H. Joe, "Molecular docking, photocatalytic activity and biomedical investigations of some metal complexes," *Journal of Biomolecular Structure and Dynamics*, vol. 39, no. 15, pp. 5600–5612, 2021.

[28] A. Chauhan, S. Saini, R. Kumar, D. Kumar, and R. Langyan, "Luminescence features of mononuclear Sm (III) complexes with heterocyclic ligands," *Optik*, vol. 231, Article ID 166500, 2021.

[29] D. Zhu and Q. Zhou, "Nitrogen doped g-C_3N_4 with the extremely narrow band gap for excellent photocatalytic activities under visible light," *Applied Catalysis B: Environmental*, vol. 281, Article ID 119474, 2021.

[30] G. Kaur, Y. Dwivedi, and S. Rai, "Synthesis, structural, thermal and optical studies of rare earth coordinated complex: $(Tb(Sal)_3Phen)$," *Materials Chemistry and Physics*, vol. 130, no. 3, pp. 1351–1356, 2011.

[31] B. Kumar, G. Kaur, and S. Rai, "Acetylsalicylic acid sensitized lasing luminescence of terbium complex in PVA: a case of energy avalanche via 1, 10-Phenanthroline," *Journal of Photochemistry and Photobiology A: Chemistry*, vol. 332, pp. 413–421, 2017.

[32] H. Singh and K. K. Bamzai, "Effect of glycine on structural, optical and dielectric properties of solution grown samarium chloride coordinated with salicylic acid," *Journal of Materials Science: Materials in Electronics*, vol. 30, no. 4, pp. 3833–3846, 2019.

[33] L. Zapała, M. Kosińska, E. Woźnicka, Ł. Byczyński, W. Zapała, and J. Kalembkiewicz, "Preparation, spectral properties and thermal decomposition of new ternary complexes of La (III), Ce (III), Pr (III) and Nd (III) ions with N-phenylanthranilic acid and 1, 10-phenanthroline," *Thermochimica Acta*, vol. 659, pp. 242–252, 2018.

[34] A. Kumar and G. Pandey, "A review on the factors affecting the photocatalytic degradation of hazardous materials," *Material Science & Engineering International Journal*, vol. 1, no. 3, pp. 1–10, 2017.

[35] G. Rajam K, S. Daravath, V. K Narendrula, P. Marri, and Shivaraj, "Synthesis, characterization, docking and antimicrobial activity studies of binuclear Co(II) and Ni(II) complexes of bisaroylhydrazone and phenanthroline," *Bulletin of the Chemical Society of Ethiopia*, vol. 35, no. 3, pp. 499–511, 2022.

[36] A. Afzaal and M. A. Farrukh, "Zwitterionic surfactant assisted synthesis of Fe doped SnO_2-SiO_2 nanocomposite with enhanced photocatalytic activity under sun light," *Materials Science and Engineering: B*, vol. 223, pp. 167–177, 2017.

[37] H. Huang, Y. Wu, S. Cheng et al., "A bismuth (III) complex ((1, 10-phen) Bi $(C_2O_4)_{1.5}$): synthesis, crystal structure and optical properties," *Inorganica Chimica Acta*, vol. 542, Article ID 121115, 2022.

[38] S. H. Tan, Z. H. Chen, H. Luo, T. Liu, and G. Q. Zhong, "Synthesis, crystal structure and photocatalytic properties of two Bismuth(III) complexes with different N-containing heterocycles," *Polyhedron*, vol. 218, Article ID 115768, 2022.

[39] H. Y. Shen, W. M. Wang, Y. X. Bi, H. L. Gao, S. Liu, and J. Z. Cui, "Luminescence, magnetocaloric effect and single-molecule magnet behavior in lanthanide complexes based on a tridentate ligand derived from 8-hydroxyquinoline," *Dalton Transactions*, vol. 44, no. 43, pp. 18893–18901, 2015.

[40] M. E. Fortună, L. Pricop, M. Zaltariov et al., "Cu (II)/Guanidine functionalized disiloxane complex of supramolecular structures for visible light-driven photocatalysis of Congo red," *Polymers*, vol. 14, no. 4, p. 817, 2022.

[41] S. S. Carvalho, A. C. C. Rodrigues, J. F. Lima, and N. M. Carvalho, "Photocatalytic degradation of dyes by mononuclear copper (II) complexes from bis-(2-pyridylmethyl) amine NNN-derivative ligands," *Inorganica Chimica Acta*, vol. 512, Article ID 119924, 2020.

[42] M. Ahmad and K. A. Siddiqui, "Synthesis of mixed ligand 3D cobalt MOFs: smart responsiveness towards photocatalytic dye degradation in environmental contaminants," *Journal of Molecular Structure*, vol. 1265, Article ID 133399, 2022.

[43] A. M. Tayeb, D. S. Hussein, and R. Farouq, "Optimization of photocatalytic degradation of methylene blue dye using titanate nanotube," *Journal of Nanophotonics*, vol. 14, no. 02, 2020.

[44] N. P. De Moraes, F. N. Silva, M. L. C. P. da Silva, T. M. B. Campos, G. P. Thim, and L. A. Rodrigues, "Methylene blue photodegradation employing hexagonal prism-shaped niobium oxide as heterogeneous catalyst: effect of catalyst dosage, dye concentration, and radiation source," *Materials Chemistry and Physics*, vol. 214, pp. 95–106, 2018.

[45] M. Jamil, Z. S. Khan, A. Ali, and N. Iqbal, "Studies on solution processed Graphene-Nb_2O_5 nanocomposite based

photoanode for dye-sensitized solar cells," *Journal of Alloys and Compounds*, vol. 694, pp. 401–407, 2017.

[46] I. Ullah, A. Haider, N. Khalid et al., "Tuning the band gap of TiO_2 by tungsten doping for efficient UV and visible photodegradation of Congo red dye," *Spectrochimica Acta Part A: Molecular and Biomolecular Spectroscopy*, vol. 204, pp. 150–157, 2018.

[47] N. Yahya, F. Aziz, J. Jaafar et al., "Impacts of annealing temperature on morphological, optical and photocatalytic properties of gel-combustion-derived $LaFeO_3$ nanoparticles," *Arabian Journal for Science and Engineering*, vol. 46, no. 7, pp. 6153–6165, 2021.

[48] M. R. Abhilash, G. Akshatha, and S. Srikantaswamy, "Photocatalytic dye degradation and biological activities of the Fe_2O_3/Cu_2O nanocomposite," *RSC Advances*, vol. 9, no. 15, pp. 8557–8568, 2019.

[49] E. E. Al-Abodi and A. Hashim, "Photo degradation of Congo red dye by using new nanocomposite," *Annals of the Romanian Society for Cell Biology*, vol. 25, no. 3, pp. 6822–6835, 2021.

[50] M. Saeed, M. Muneer, N. Akram, A. Ul Haq, N. Afzal, and M. Hamayun, "Synthesis and characterization of silver loaded alumina and evaluation of its photo catalytic activity on photodegradation of methylene blue dye," *Chemical Engineering Research and Design*, vol. 148, pp. 218–226, 2019.

[51] Y. W. Chen and Y. H. Hsu, "Effects of reaction temperature on the photocatalytic activity of TiO_2 with Pd and Cu cocatalysts," *Catalysts*, vol. 11, no. 8, p. 966, 2021.

[52] A. Salama, A. Mohamed, N. M. Aboamera, T. A. Osman, and A. Khattab, "Photocatalytic degradation of organic dyes using composite nanofibers under UV irradiation," *Applied Nanoscience*, vol. 8, no. 1-2, pp. 155–161, 2018.

[53] H. Luo, R. G. Yang, Z. H. Chen, and G. Q. Zhong, "Three Bismuth(III) complexes constructed by N-containing heterocyclic carboxylic acids: synthesis, crystal structure and photocatalytic activity," *Journal of Solid State Chemistry*, vol. 300, Article ID 122256, 2021.